

DUST TEMPERATURES IN THE *INFRARED SPACE OBSERVATORY* ATLAS OF BRIGHT SPIRAL GALAXIES¹

GEORGE J. BENDO,^{2,3,4} ROBERT D. JOSEPH,³ MARTYN WELLS,⁵ PASCAL GALLAIS,⁶ MARTIN HAAS,⁷ ANA M. HERAS,^{8,9}
ULRICH KLAAS,⁷ RENÉ J. LAUREIJS,^{8,9} KIERON LEECH,^{9,10} DIETRICH LEMKE,⁷ LEO METCALFE,⁸
MICHAEL ROWAN-ROBINSON,¹¹ BERNHARD SCHULZ,^{9,12} AND CHARLES TELESKO¹³

Received 2002 May 23; accepted 2003 January 24

ABSTRACT

We examine far-infrared and submillimeter spectral energy distributions for galaxies in the *Infrared Space Observatory* Atlas of Bright Spiral Galaxies. For the 71 galaxies where we had complete 60–180 μm data, we fitted blackbodies with λ^{-1} emissivities and average temperatures of 31 K or λ^{-2} emissivities and average temperatures of 22 K. Except for high temperatures determined in some early-type galaxies, the temperatures show no dependence on any galaxy characteristic. For the 60–850 μm range in eight galaxies, we fitted blackbodies with λ^{-1} , λ^{-2} , and $\lambda^{-\beta}$ (with β variable) emissivities to the data. The best results were with the $\lambda^{-\beta}$ emissivities, where the temperatures were ~ 30 K and the emissivity coefficient β ranged from 0.9 to 1.9. These results produced gas-to-dust ratios that ranged from 150 to 580, which were consistent with the ratio for the Milky Way and which exhibited relatively little dispersion compared with fits with fixed emissivities.

Key words: dust, extinction — galaxies: ISM — galaxies: spiral

1. INTRODUCTION

The far-infrared emission from galaxies is emitted by interstellar dust heated by a variety of energy sources. Two important energy sources are the general interstellar radiation field and the more intense radiation in star formation regions. These should produce dust sources at different dust temperatures and with different spatial distributions. Understanding these dust temperature components is necessary for understanding the relation between far-infrared emission and star formation in galaxies.

While much of the research in this subject has focused on ultraluminous galaxies and high-redshift objects, some studies have investigated dust temperatures in normal spiral galaxies. However, no clear consensus has been reached on the temperatures of the dust components in spiral galaxies. Perhaps the most contentious issue is whether a significant dust component at a very low temperature, ~ 10 – 15 K, exists. This issue needs to be resolved to understand how the interstellar radiation field and star formation regions heat dust to produce far-infrared emission.

Before the launch of the *Infrared Space Observatory* (*ISO*; Kessler et al. 1996), most research on dust temperatures in galaxies relied on combining *IRAS* or Kuiper Airborne Observatory (KAO) data with ground-based submillimeter or millimeter data. The launch of *ISO* has permitted better far-infrared spectral energy distributions to be measured.

Smith (1982) was the first to measure a dust temperature in a nonactive spiral. Using KAO data, he found a temperature of 20 K in NGC 5194 (M51). Chini et al. (1986) combined submillimeter bolometer data from NASA's Infrared Telescope Facility (IRTF) with *IRAS* far-infrared data to conclude that spiral galaxies have cold dust components with an average temperature of 16 K. Stark et al. (1989) measured far-infrared fluxes with the KAO and submillimeter fluxes with the NASA IRTF for three Virgo Cluster spirals and inferred significantly warmer dust temperatures than those determined by Chini et al. (1986). Eales, Wynn-Williams, & Duncan (1989) measured dust temperatures in 11 galaxies using *IRAS* far-infrared data and submillimeter bolometer data from UKIRT and determined that the coolest dust component in spiral galaxies was 30–50 K, much warmer than previous measurements. These studies thus established a controversy over the apparently simple issue of the dust temperatures in spiral galaxies.

Subsequent studies have produced similarly conflicting results. Most have focused on individual galaxies, including NGC 660, UGC 3490 (Chini & Krügel 1993), NGC 3267 (Sievers et al. 1994), NGC 4631 (Braine et al. 1995), M51

¹ Based on observations with *Infrared Space Observatory*, an ESA project with instruments funded by ESA Member States (especially the PI countries: France, Germany, the Netherlands, and the United Kingdom) and with the participation of ISAS and NASA.

² Steward Observatory, University of Arizona, 933 North Cherry Avenue, Tucson, AZ 85721; gbendo@as.arizona.edu.

³ Institute for Astronomy, University of Hawaii, 2680 Woodlawn Drive, Honolulu, HI 96822; joseph@ifa.hawaii.edu.

⁴ Guest User, Canadian Astronomy Data Centre, which is operated by the Dominion Astrophysical Observatory for the National Research Council of Canada's Herzberg Institute of Astrophysics.

⁵ UK Astronomy Technology Centre, Royal Observatory Edinburgh, Blackford Hill, Edinburgh EH9 3HJ, Scotland, UK; mw@roe.ac.uk.

⁶ CEA/DSM/DAPNIA Service d'Astrophysique, F-91191 Gif-sur-Yvette, France; gallais@discovery.saclay.cea.fr.

⁷ Max-Planck-Institut für Astronomie, Königstuhl 17, D-69117 Heidelberg, Germany; haas@mpia-hd.mpg.de, klaas@mpia-hd.mpg.de, lemke@mpia-hd.mpg.de.

⁸ Astrophysics Division, Space Science Department of ESA, ESTEC, P.O. Box 299, 2200 AG Noordwijk, Netherlands; aheras@estsat2.estec.esa.nl, rlaureij@rssd.esa.int.

⁹ *ISO* Data Center, Astrophysics Division, ESA, Villafranca de Castillo, E-28080 Madrid, Spain; lmetcalf@iso.vilspa.esa.es.

¹⁰ Said Business School, Park End Street, Oxford OX1 1HP, England, UK; kieron.leech@said-business-school.oxford.ac.uk.

¹¹ Astrophysics Group, Imperial College, Blackett Laboratory, Prince Consort Road, London SW7 2BZ, England, UK; m.rrobinson@ic.ac.uk.

¹² Infrared Processing and Analysis Center, MS 100-22, California Institute of Technology, 770 South Wilson Avenue, Pasadena, CA 91125; bschulz@ipac.caltech.edu.

¹³ Department of Astronomy, University of Florida, P.O. Box 112055, Gainesville, FL 32611; telesco@astro.ufl.edu.

(Guèlin et al. 1995; Hippelein et al. 1996), M101 (Hippelein et al. 1996), the Andromeda Galaxy (Haas et al. 1998), and NGC 891 (Popescu et al. 2000). These studies typically find dust temperatures of ~ 20 K, with the lowest temperature being 16 K and the highest being 33 K. There have been a few studies of larger samples. Some of these surveys have found far-infrared dust temperatures as high as 35 K (Clements, Andreani, & Chase 1993; Dunne et al. 2000). Others have found temperatures between 20 and 30 K (Dunne & Eales 2001; Popescu et al. 2002), and still others have found dust components as cold as 10–15 K (Chini et al. 1995; Krügel et al. 1998; Siebenmorgen, Krügel, & Chini 1999; Stickel et al. 2000).

Part of the reason no consensus has been reached on dust temperatures in normal galaxies is because of poor sampling of the spectral energy distribution (SED). To find reliable dust temperatures, it is vital to evenly sample the SEDs from the Wien side to the Rayleigh-Jeans side of the Planck spectrum. Some studies have had such poor spectral sampling that Planck functions are fitted to data with no degrees of freedom, and some have entire dust temperature components defined by a single measurement. Another source of the discrepancy is that different studies assume different wavelength dependences for the emissivity. In general, when a shallower emissivity function is chosen, this produces warmer temperatures.

In this paper, we combine far-infrared *ISO* photometry with submillimeter photometry from the Submillimetre Common-User Bolometer Array (SCUBA; Holland et al. 1999) at the James Clerk Maxwell Telescope (JCMT) to sample the full spectrum of cool dust emission in normal spiral galaxies. We will first present the dust temperatures we infer from 60, 100, and 180 μm *ISO* measurements for 71 spiral galaxies in the *ISO* Atlas of Bright Spiral Galaxies (Bendo et al. 2002, henceforth referred to as Paper I). We then examine dust temperatures obtained by combining the far-infrared data with submillimeter data for eight of the galaxies in the sample. Finally, we calculate dust masses and examine gas-to-dust mass ratios for seven of these galaxies.

2. DATA

2.1. The Sample

The galaxies in this sample are a subset of a complete, magnitude-limited set of galaxies selected from the Revised Shapley-Ames (RSA) Catalog (Sandage & Tammann 1987). The sample comprised galaxies with Hubble types between S0 and Sd and with magnitudes $B_T = 12$ or brighter; galaxies in the Virgo Cluster were excluded. A randomly selected, subset of these galaxies was observed by *ISO* based on target visibility. This produced a total of 77 galaxies that are representative of the range of Hubble types in the RSA Catalog, 71 of which were observed successfully with ISOPHOT. Detailed information on the sample is presented in Paper I.

2.2. Observations and Data Analysis

2.2.1. Far-Infrared Photometry

The 60, 100, and 180 μm photometric data were taken with ISOPHOT (Lemke et al. 1996) and processed with PIA 8.0 (Gabriel et al. 1997) with additional processing to correct for PSF effects, as discussed in Paper I. Note that, for the analysis without the submillimeter data, we assume that

the 180 μm flux within the 180'' apertures effectively comes from the same sources as the 60 and 100 μm fluxes within a 135'' aperture. To investigate how much extra far-infrared flux may come from the region outside the 135'' aperture but within the 180'' aperture, we investigated the distribution of infrared flux in maps of *IRAS* data made by the HIRES software package provided by the Infrared Processing and Analysis Center. We find that the median ratio of flux within 135'' to flux within 180'' is 0.85 at 60 μm and 0.80 at 100 μm for the galaxies in this sample. According to the HIRES beam profiles, point sources would have ratios of 0.95 at 60 μm and 0.85 at 100 μm . The small difference between the ratio of fluxes for the sample galaxies and the ratio expected for point sources suggests that most of the emission between the 135'' and 180'' apertures in the HIRES maps is mostly from the point-spread function, and that emission in those regions is relatively small in most galaxies. We will assume that the distribution of the 180 μm emission will be similar to the 100 μm emission, so therefore, we will assert that most of the 180 μm emission for the galaxies in this sample also comes from within 135''. When we also have submillimeter data, however, we can make assumptions about the spatial distribution of the emission and perform a deconvolution analysis to estimate the 180 μm fluxes within 45'' and 135'' apertures.

2.2.2. Submillimeter Photometry

We observed NGC 4088 and NGC 4826 at 850 μm using SCUBA at the JCMT. The data were taken in jiggle map mode, in which the telescope's secondary mirror shifts in a 64-point pattern to create a completely sampled map for the inner 135'' of the target. For sky subtraction, we nodded 2' off-source parallel to the optical disks' minor axes for each galaxy. Integration times were 64 minutes for NGC 4088 and 60 minutes for NGC 4826. We performed sky dips regularly to check the opacity during the observations. At 850 μm , the opacity typically ranged between 0.3 and 0.6 for all the observations. (The high sky opacity made the simultaneous 450 μm observations useless.) For calibration, we observed Mars using similar methods.

In addition to the above data, we have used data from the JCMT SCUBA archives for six galaxies: NGC 4414, 4631, 5236, 5713, 5792, and 5907. All of these data were taken in SCUBA's jiggle map mode, with either Uranus, OH 231.8, or IRC +10216 used for calibration.

The data were processed with the SCUBA User Reduction Facility (Jenness & Lightfoot 1998) following the typical processing steps. First, the data were flat-fielded and corrected for air mass and sky opacity. Bad bolometers were flagged and masked. An additional background selection was made by measuring and subtracting surface brightnesses in selected off-target bolometers using the "remsky" procedure. Finally, the data were combined together and rebinned to produce final maps. Images of planets and other calibration sources were processed using the same methods. Signals were measured within 45'' and 135'' apertures, which are comparable to the apertures of ISOPHOT. For calibration, we measured the signals from the standard sources in similarly sized apertures, and these then provided conversion factors for converting signals to flux densities for the targets. We assume that the uncertainty in both the new measurements and the archival measurements comes primarily from the uncertainty in the calibration, which is

TABLE 1
SUBMILLIMETER FLUX DENSITY MEASUREMENTS

GALAXY	450 μm FLUX DENSITY (Jy)		850 μm FLUX DENSITY (Jy)		$\log \log D_{25}^a$	DATA SOURCE
	45''	135''	45''	135''		
NGC 4088.....	0.26 ± 0.03	0.98 ± 0.10	1.76	Observation
NGC 4414.....	2.8 ± 0.3	7.3 ± 0.7	0.36 ± 0.04	0.84 ± 0.08	1.56	Archive
NGC 4631.....	4.8 ± 0.5	18 ± 0.2	0.54 ± 0.05	1.89 ± 0.19	2.19	Archive
NGC 4826.....	0.63 ± 0.06	1.01 ± 0.10	2.00	Observation
NGC 5236.....	5.5 ± 0.5	9.7 ± 0.9	0.82 ± 0.08	1.36 ± 0.14	2.11	Archive
NGC 5713.....	0.26 ± 0.03	0.43 ± 0.04	1.44	Archive
NGC 5792.....	0.18 ± 0.02	0.33 ± 0.03	1.84	Archive
NGC 5907.....	0.43 ± 0.04	1.26 ± 0.13	2.10	Archive

^a The optical diameter parameter defined in de Vaucouleurs et al. 1991.

approximately 10%. Other sources of uncertainty, mainly uncertainties from background noise, appear to be less significant. Table 1 lists the resulting flux densities, as well as the optical diameter parameter from the Third Reference Catalogue of Bright Galaxies (de Vaucouleurs et al. 1991), and an indication of whether the data came from original observations or the JCMT SCUBA archives.

3. SPECTRAL ENERGY DISTRIBUTIONS AND DUST TEMPERATURES

3.1. Far-Infrared Spectral Energy Distributions

First, we fitted blackbody functions with two different emissivity functions to the data. The emissivity functions we selected scale as λ^{-1} and λ^{-2} , functions that are used by many studies cited in § 1 and that are recommended by Hildebrand (1983).

Table 2 lists the dust temperatures determined from the *ISO* far-infrared data, and Figure 1 shows histograms of these temperatures. We estimate an error of ~ 2 K in the dust temperatures due to uncertainties in the photometric calibration of ISOPHOT. This error was determined by fitting blackbodies to data where the 60 μm flux was increased 20% and the 180 μm flux was decreased 20% and vice versa. The temperatures of the fits are, for the λ^{-1}

emissivity, a mean of 31 K with a range of 24–42 K and, for the λ^{-2} emissivity, a mean of 25 K with a range of 21–32 K. The functions with the λ^{-1} emissivities generally fit the data better according to the χ^2 criterion.

The dust temperatures vary little in relation to morphology and active galactic nuclei activity. The data in Table 3 do show that some S0 and elliptical galaxies tend to have warmer dust temperatures, but all the spiral and irregular galaxies have indistinguishable dust temperatures.

These results should be compared with those of Stickel et al. (2000), who used *IRAS* 60 and 100 μm data supplemented by 170 μm photometry from the *ISO* Serendipity Survey for 115 galaxies. They assumed an emissivity function scaling as λ^{-2} and found a temperature distribution centered at 20 K with a range of 15–25 K. These results are systematically colder by 5–6 K, and they conclude that “for the first time this indicates that a cold dust component with $T_D \leq 20$ K is present in a large fraction of all spiral galaxies.” In contrast, using the same emissivity function, we find no galaxy with $T_D < 21$ K and no support for such a cold dust component in most spiral galaxies. One possible explanation could be that Stickel et al. (2000) use *IRAS* Faint Source Catalog (FSC) data at 60 and 100 μm , whereas we have used *ISO* photometry at 60 and 100 μm and were able to make approximate corrections for the point-spread

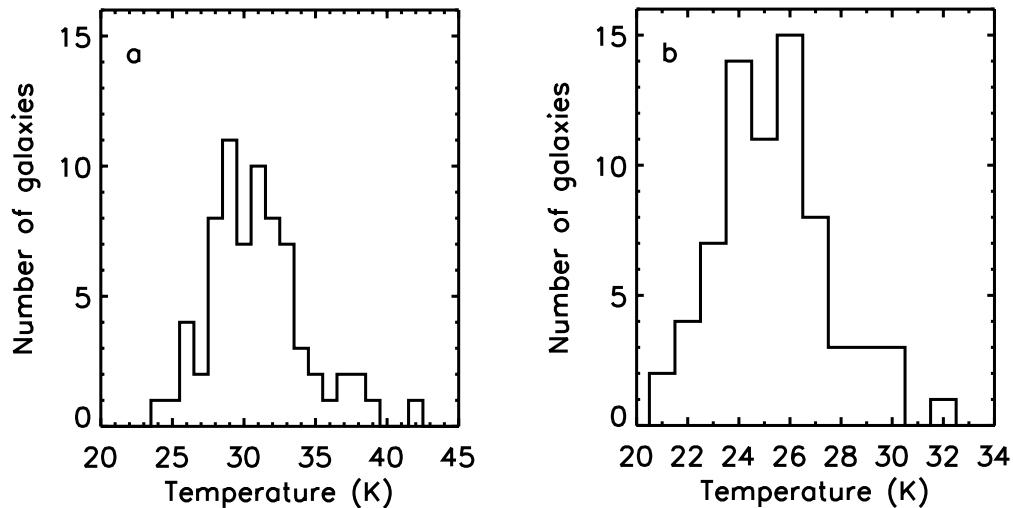


FIG. 1.—Histograms of the temperatures with (a) λ^{-1} and (b) λ^{-2} emissivities, as determined from the 60–180 μm data

TABLE 2
TEMPERATURES FROM FAR-INFRARED SEDs

GALAXY	TEMPERATURE (K) ^a	
	λ^{-1} Emissivity	λ^{-2} Emissivity
NGC 55.....	26	22
NGC 289.....	31	25
NGC 1512.....	31	26
NGC 3359.....	32	26
NGC 3556.....	31	26
NGC 3898.....	30	25
NGC 4062.....	28	23
NGC 4088.....	31	25
NGC 4096.....	29	24
NGC 4100.....	33	26
NGC 4136.....	30	25
NGC 4157.....	29	24
NGC 4203.....	32	26
NGC 4236.....	32	26
NGC 4244.....	27	23
NGC 4274.....	29	24
NGC 4314.....	34	28
NGC 4395.....	26	22
NGC 4414.....	31	25
NGC 4448.....	30	25
NGC 4559.....	29	24
NGC 4605.....	32	26
NGC 4618.....	30	25
NGC 4631.....	34	27
NGC 4710.....	33	27
NGC 4725.....	24	21
NGC 4826.....	33	27
NGC 4984.....	39	30
NGC 5033.....	30	25
NGC 5054.....	31	26
NGC 5055.....	28	24
NGC 5087.....	38	30
NGC 5101.....	28	24
NGC 5102.....	29	24
NGC 5112.....	29	24
NGC 5170.....	28	24
NGC 5204.....	33	27
NGC 5236.....	36	29
NGC 5247.....	29	24
NGC 5300.....	29	24
NGC 5334.....	28	23
NGC 5364.....	26	22
NGC 5371.....	28	23
NGC 5457.....	27	23
NGC 5474.....	32	26
NGC 5556.....	33	27
NGC 5566.....	29	24
NGC 5584.....	32	26
NGC 5585.....	33	27
NGC 5669.....	29	24
NGC 5676.....	31	26
NGC 5701.....	31	25
NGC 5713.....	37	29
NGC 5746.....	28	23
NGC 5792.....	33	27
NGC 5838.....	42	32
NGC 5846.....	37	29
NGC 5850.....	30	25
NGC 5866.....	32	26
NGC 5907.....	26	22
NGC 5985.....	28	23
NGC 6015.....	29	24
NGC 6215.....	35	28

TABLE 2—Continued

GALAXY	TEMPERATURE (K) ^a	
	λ^{-1} Emissivity	λ^{-2} Emissivity
NGC 6217.....	35	28
NGC 6221.....	34	27
NGC 6300.....	31	26
NGC 6340.....	38	30
NGC 6503.....	30	25
NGC 6643.....	31	26
NGC 6744.....	25	21
NGC 6753.....	32	26

^a Errors on the temperature measurements are 2 K.

function. As we demonstrated in Paper I, the *ISO* fluxes used in this research, particularly the 60 μm fluxes, are systematically higher than those in the *IRAS* FSC, which would naturally lead to the temperatures found using the *ISO* photometry to be higher than those found using corresponding *IRAS* FSC data.

However, some qualifications must be made to interpretations based on data confined to this relatively small wavelength range, even though these data from *ISO* include the longer wavelength 180 μm measurement that *IRAS* did not have. First, if dust components 10–15 K exist, their contribution would not be evident using the far-infrared data alone. Second, emission at 60 μm may include emission from warmer dust components that cause the SED to flatten out (see Laureijs et al. 2000 for an example based on observational data of galactic cirrus, Popescu et al. 2000 and Dunne & Eales 2001 for examples of blackbody fits to observations of nearby galaxies, or Désert, Boulanger, & Puget 1990 and Dale et al. 2001 for detailed modeling of dust emission at far-infrared wavelengths). Thus, fitting single blackbody functions through the 60, 100, and 180 μm data points is possible but may not accurately describe the physics of the dust emission. The addition of longer wavelength data may provide evidence for more than one dust component. Therefore, in the next section, we examine the blackbody fits obtained when the far-infrared data are combined with submillimeter data.

3.2. Far-Infrared to Submillimeter Spectral Energy Distributions

We have submillimeter and far-infrared data for a subset of eight of the *ISO* galaxy sample, and blackbody functions

TABLE 3
DEPENDENCE OF FAR-INFRARED DUST TEMPERATURES ON MORPHOLOGICAL TYPE

MORPHOLOGICAL TYPE	NUMBER	MEAN TEMPERATURES (K)	
		With λ^{-1} Emissivity	With λ^{-2} Emissivity
All.....	71	30.9 \pm 0.4	25.3 \pm 0.3
E–S0/a.....	11	34.5 \pm 1.4	27.5 \pm 0.8
Sa–Sab.....	8	30.0 \pm 1.1	25.0 \pm 0.8
Sb–Sbc.....	19	30.3 \pm 0.7	24.9 \pm 0.5
Sc–Scd.....	25	30.2 \pm 0.5	24.9 \pm 0.3
Sd–Irr.....	8	30.9 \pm 1.1	25.4 \pm 0.8

with λ^{-1} and $\lambda^{-\beta}$ emissivities, with β variable, have been fitted to these data. We refer to the resulting dust temperatures measured within 135'' apertures as global dust temperatures. We also determined the temperatures of dust within the inner 45'' of the galaxies, and we refer to these as the nuclear dust temperatures. (We note our designation “nuclear” is very qualitative; at the distances of these galaxies, 45'' subtends ≥ 1 kpc, a much larger region than would normally be considered the galaxy nucleus. Starburst regions in galaxies are typically 250–500 pc.) The dust temperatures measured within a 135'' aperture but outside a 45'' aperture we refer to as disk temperatures. These distinctions permit investigation of the differences between dust temperatures in the inner and outer regions of these galaxies.

Since the diffraction limit of the *ISO* telescope at 180 μm is $\sim 145''$, to do this analysis for the 180 μm data requires estimating the fluxes from both central unresolved and extended components. We use a method similar to that used by Radovich et al. (1999). (We also used this method for the 60 and 100 μm data in Paper I.) We calculate the ratio of fluxes for the point and extended sources at both 100 and 850 μm , since we have the required 45'' resolution at both these wavelengths. We then interpolate to estimate the ratio of the 180 μm fluxes from point and extended components. According to Laureijs (1999)¹⁴, 61.2% of the flux from a point source centered in the C200 array (the 180 μm measurement) will fall on the array. Therefore, the flux within the 180'' aperture can be expressed as

$$f_m(180'') = 0.612f_c + (180'')^2 f_e, \quad (1)$$

where f_m is the measured flux, f_c is the flux from the central source, and f_e is the flux arcsec⁻² from a diffuse, uniform, extended source. Substituting the ratio $f_c/[(180'')^2 f_e]$ into the above equation allows for solving for f_c and f_e :

$$f_c = \frac{f_m}{0.612 + \{[(180'')^2 f_e]/f_c\}}, \quad (2)$$

$$f_e = \frac{f_m}{0.612\{f_c/[(180'')^2 f_e]\} + 1}. \quad (3)$$

These central and extended components can then be used to calculate fluxes within 45'' and 135'' apertures:

$$f_i(45'') = f_c + (45'')^2 f_e, \quad (4)$$

$$f_i(135'') = f_c + (135'')^2 f_e. \quad (5)$$

The resulting 180 μm flux densities are listed in Table 4. We can now use these 180 μm flux estimates for the dust temperature analysis outlined above.

Table 5 lists the resulting dust temperatures derived using the λ^{-1} emissivities, and Table 6 lists the dust temperatures for $\lambda^{-\beta}$ emissivities. In addition, Figures 2–9 show the SEDs and the fits of blackbody functions with $\lambda^{-\beta}$ emissivities. We also tried fitting single blackbodies with λ^{-2} emissivities to the data, but except for NGC 5236 (which will be discussed below) the fits were very poor. We estimated an error of ~ 1 K in these dust temperatures using the same method described above for the far-infrared SEDs. In summary, the

fits yield dust temperatures of ~ 35 K for models with λ^{-1} emissivities and ~ 30 K for models with $\lambda^{-\beta}$ emissivities. Typical fits to the emissivity coefficient were between 0.9 and 1.4.

NGC 5236 is exceptional in that the emissivity function is closer to λ^{-2} . NGC 5236 is a galaxy with unusual supernova activity. Shocks from the strong supernova activity associated with the galaxy's nucleus could be responsible for breaking up larger dust grains into smaller grains, thus making the wavelength dependence of the emissivity function steeper. The disk of NGC 4414, but not the nucleus, also exhibits a steep emissivity. Star formation has been inhibited in the nucleus by the lack of molecular gas present (Sakamoto 1996), but sites of strong star formation are evident in the disk (cf. Fig. 25 in Paper I), and the large dust grains may have suffered similar fragmentation as in NGC 5236.

In general, the “nuclear” dust temperatures are systematically warmer than the disk temperatures in all cases. Because stellar densities are higher in the nuclei of these galaxies, and because the star formation rate may be higher, the interstellar radiation field is stronger. This enhances both the dust emission and the dust temperatures, producing the observed differences in dust temperatures between the nuclear and disk regions.

Since some other studies have suggested there are two temperature components, we have also investigated the possibility that the dust emission may be composed of two blackbody components. This obviously requires steeper wavelength dependence for the emissivities. We therefore chose emissivity functions proportional to λ^{-2} for both temperature components. Table 7 shows the best-fitting temperatures, with two temperatures derived for all galaxies except NGC 5236. (For NGC 5236, the analysis demonstrates that a second blackbody component would make only a minor contribution to the far-infrared and submillimeter SED, so only one component was fitted to the data.) In most cases, the two components have temperatures of ~ 15 and ~ 30 K. For galaxies with no 450 μm data, the solution is an even-determined problem with an exact fit that should be interpreted with caution. Moreover, the colder dust temperature is dependent mainly on the submillimeter measurement, so errors in the submillimeter measurement directly affect the temperature of the coldest component.

Having used submillimeter data to determine dust temperatures for these eight galaxies, we can now compare the temperatures found for these same galaxies used the *ISO* far-infrared data alone. Comparing the dust temperatures in Table 2 with the “Global” temperatures in Table 5 and Table 7 shows that the addition of the submillimeter data systematically increases the derived dust temperatures ~ 2 – 3 K. The more significant difference is that, by adding the submillimeter data point(s), one can search for a very cold dust component of temperature ~ 6 – 15 K.

In summary, for these eight galaxies with both *ISO* far-infrared and submillimeter measurements, we find dust temperatures in almost all cases that can be described as a ~ 35 K blackbody with a λ^{-1} emissivity, a ~ 30 K blackbody with a variable emissivity coefficient ranging from 0.9 to 1.4, or two blackbodies with temperatures of ~ 15 and ~ 30 K and λ^{-2} emissivities. Clearly, the far-infrared-to-submillimeter SEDs of galaxies can be represented with several different functions and correspondingly larger or smaller

¹⁴ Available at http://www.iso.vilspa.esa.es/users/expl_lib/PHT/c200fpsf02.ps.gz.

TABLE 4
RESULTS OF DECONVOLUTION ANALYSIS ON 180 μm DATA

GALAXY	MEASURED 180 μm FLUX DENSITIES (180'')	DECONVOLVED 180 μm FLUX DENSITIES (Jy)			
		In Components		In Set Apertures	
		Central	Extended (135'')	(45'')	(135'')
NGC 4088.....	46.2	8.4	23	11	31
NGC 4414.....	54.5	22	23	25	45
NGC 4631.....	93.9	19	46	24	65
NGC 4826.....	51.8	18	34	34	50
NGC 5236.....	192	90	77	99	170
NGC 5713.....	22.3	16	7	17	23
NGC 5792.....	15.9	8.7	6.0	9.3	15
NGC 5907.....	44.1	9.1	22	12	31

TABLE 5
TEMPERATURES WITH λ^{-1} EMISSIVITY

GALAXY	GLOBAL		NUCLEAR		Disk	
	Temperature ^a (K)	Reduced χ^2	Temperature ^a (K)	Reduced χ^2	Temperature ^a (K)	Reduced χ^2
NGC 4088.....	33	0.014	35	0.44	32	0.17
NGC 4414.....	34	3.0	35	0.95	33	12
NGC 4631.....	35	3.4	37	3.5	34	3.7
NGC 4826.....	35	2.0	36	2.2	32	2.5
NGC 5236.....	45	10	48	7.0	41	18
NGC 5713.....	39	1.6	41	2.9	34	0.64
NGC 5792.....	35	0.79	37	1.4	30	1.26
NGC 5907.....	27	0.33	28	0.46	27	0.26

^a Errors on the temperature measurements are 2 K.

TABLE 6
TEMPERATURES WITH $\lambda^{-\beta}$ EMISSIVITY

GALAXY	GLOBAL			NUCLEAR			Disk		
	Temperature ^a (K)	β	Reduced χ^2	Temperature ^a (K)	β	Reduced χ^2	Temperature ^a (K)	β	Reduced χ^2
NGC 4088.....	34	1.0	0.0055	33	1.1	0.11	34	0.9	0.0030
NGC 4414.....	29	1.4	0.52	31	1.3	0.66	26	1.7	5.4
NGC 4631.....	35	1.0	5.1	34	1.2	3.8	35	0.9	5.9
NGC 4826.....	31	1.3	0.011	32	1.3	0.11	28	1.4	0.20
NGC 5236.....	30	1.9	0.19	33	1.7	0.80	26	2.1	0.69
NGC 5713.....	34	1.3	0.022	35	1.4	0.15	31	1.2	0.32
NGC 5792.....	32	1.2	0.28	34	1.2	0.82	27	1.3	0.17
NGC 5907.....	28	0.9	0.45	29	0.9	0.83	28	0.9	0.28

^a Errors on the temperature measurements are 2 K.

TABLE 7
TEMPERATURES WITH λ^{-2} EMISSIVITY

GALAXY	GLOBAL		NUCLEAR		Disk	
	Temperature ^a (K)	Reduced χ^2	Temperature ^a (K)	Reduced χ^2	Temperature ^a (K)	Reduced χ^2
NGC 4088.....	13, 29	...	14, 30	...	12, 28	...
NGC 4414.....	15, 28	0.031	7, 27	0.70	18, 28	6.1
NGC 4631.....	12, 30	2.5	14, 31	1.9	12, 30	2.9
NGC 4826.....	14, 28	...	15, 30	...	5, 25	...
NGC 5236.....	29	0.29	30	1.6	27	0.78
NGC 5713.....	14, 31	...	16, 33	...	6, 27	...
NGC 5792.....	15, 30	...	17, 34	...	9, 24	...
NGC 5907.....	13, 26	...	14, 27	...	13, 25	...

^a Errors on the temperature measurements are 2 K.

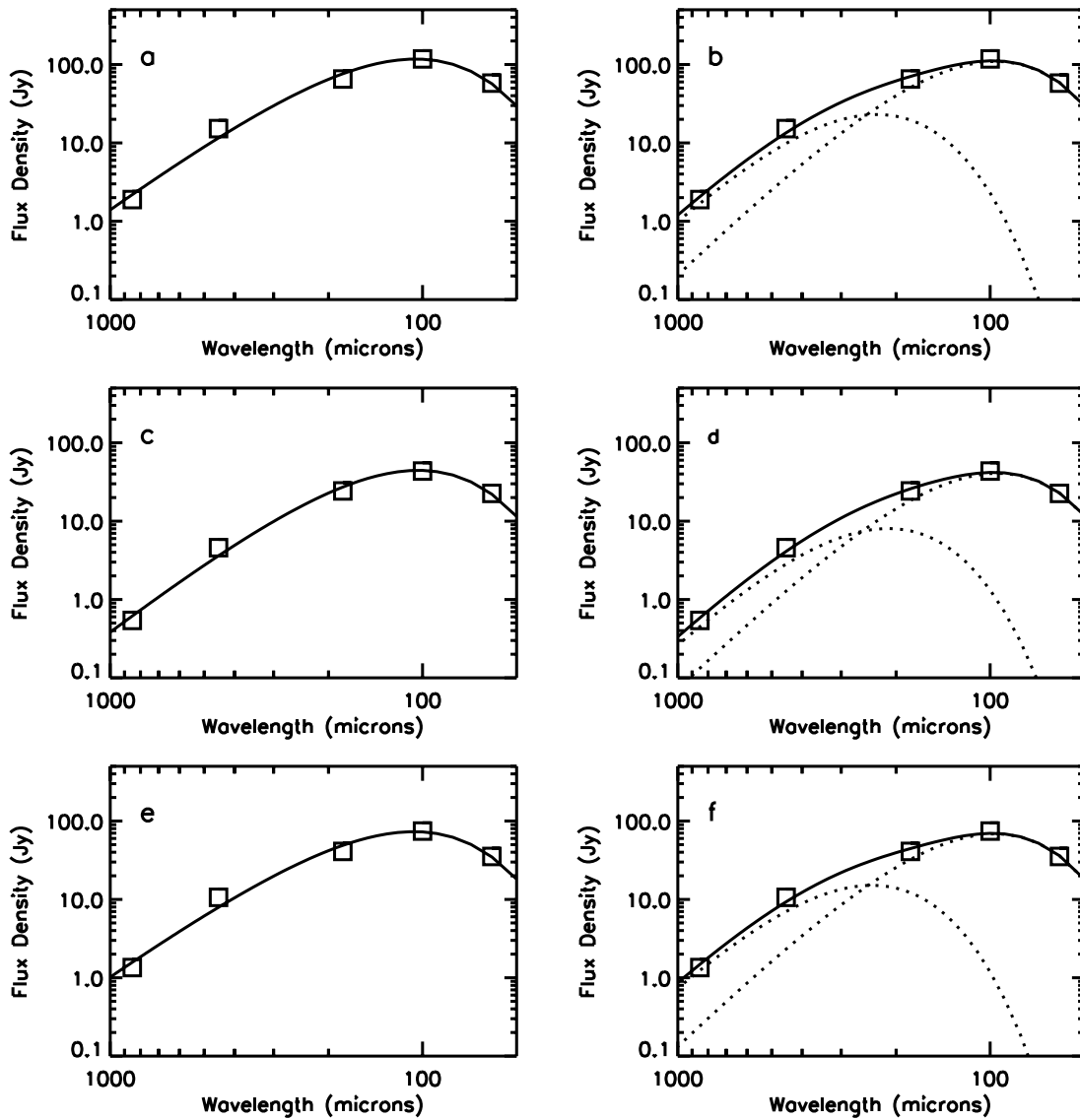


FIG. 2.—(a, b) Global, (c, d) nuclear, and (e, f) disk SEDs for NGC 4631. The measured data are represented by squares, and the errors for the data are less than the size of the squares. Parts (a), (c), and (e) show the best-fitting blackbodies with $\lambda^{-\beta}$ emissivities (with β variable). Parts (b), (d), and (f) show the best-fitting two blackbody components with λ^{-2} emissivities, with the dotted lines represent the individual blackbody components. This format also applies to Figures 3–9, although only the global SEDs are shown in those cases.

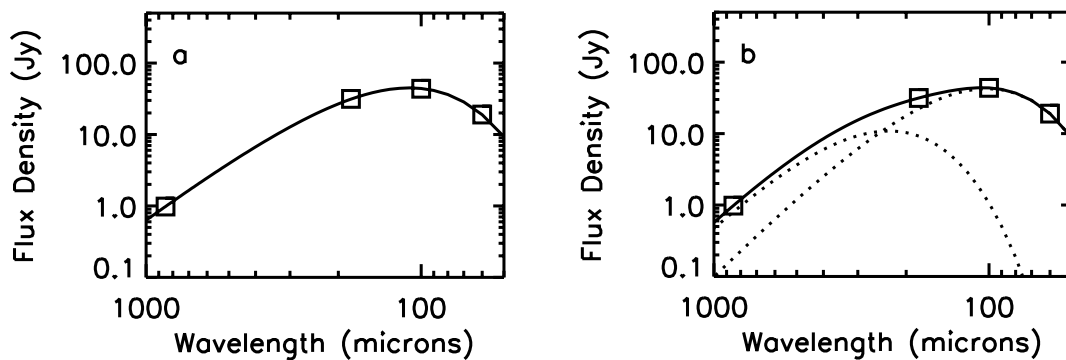


FIG. 3.—Global SED for NGC 4088

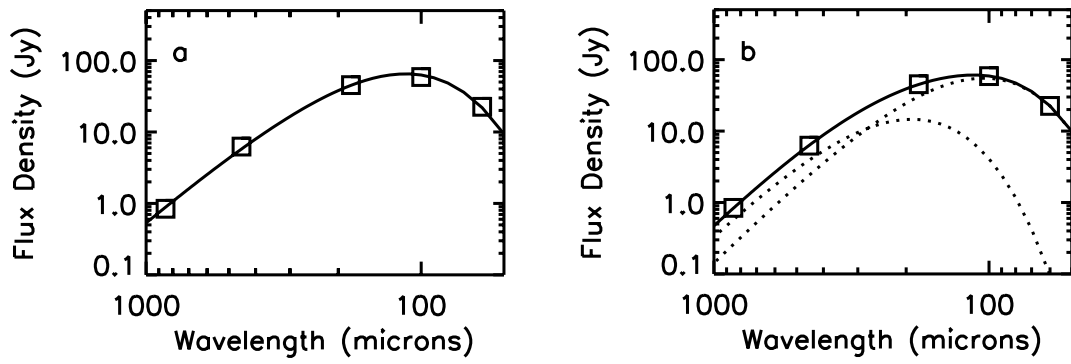


FIG. 4.—Same as Fig. 3, but for NGC 4414

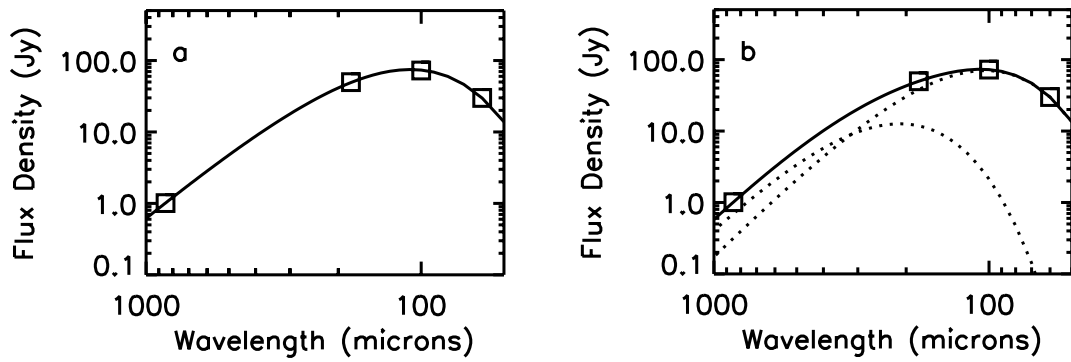


FIG. 5.—Same as Fig. 3, but for NGC 4826

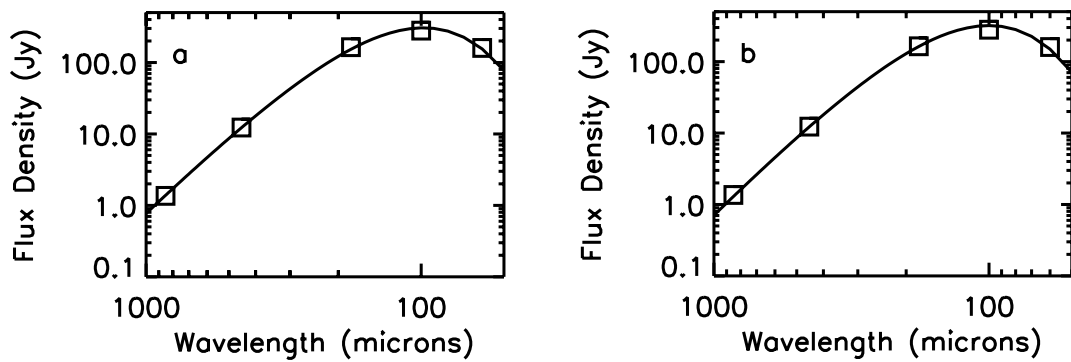


FIG. 6.—Same as Fig. 3, but for NGC 5236

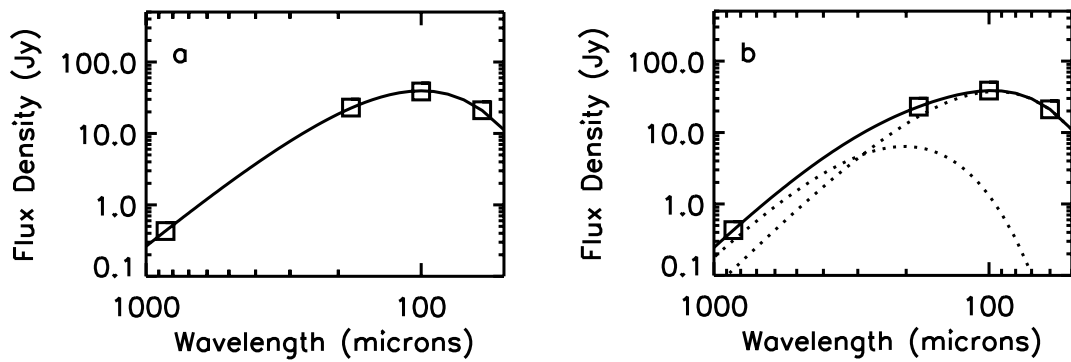


FIG. 7.—Same as Fig. 3, but for NGC 5713

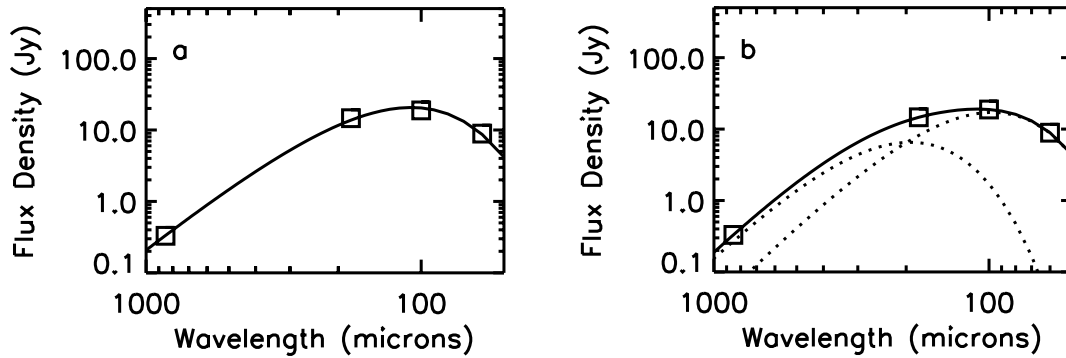


FIG. 8.—Same as Fig. 3, but for NGC 5792

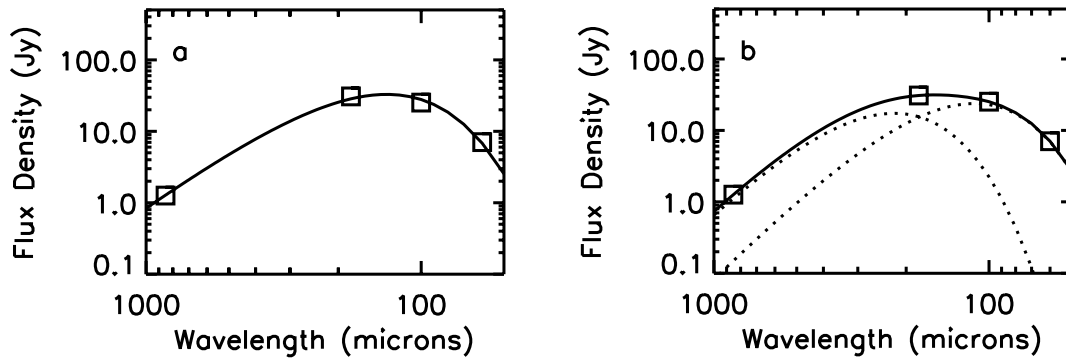


FIG. 9.—Same as Fig. 3, but for NGC 5907

dust temperatures. This is essentially a duplication of the variety of results found in the literature for the past two decades. The key question is, which of these is most likely to be correct? We return to this question in § 4.2.

4. GAS-TO-DUST MASS RATIOS

The accurate measurement of dust temperatures is not only necessary for understanding dust emission in galaxies. It is also required for measuring the gas-to-dust ratios in spiral galaxies. As discussed by Devereux & Young (1990), the temperatures and dust masses measured with *IRAS* data, when combined with molecular gas data, produced gas-to-dust mass ratios of approximately 1000. This is a factor of 10 larger than the value for the Milky Way, and it therefore raises a serious problem. This problem has also appeared in most other studies in which cold dust components have been found. The *ISO* Serendipity Survey by Stickel et al. (2000) is a notable exception; the typical gas-to-dust mass ratios found are near that of the Milky Way, but the ratios range from 50 to 1000. If these results are reliable, they raise the question whether this basic property of the interstellar medium really varies so dramatically among galaxies.

Young et al. (1995) list CO flux measurements for the eight galaxies for which we have far-infrared and submillimeter flux measurements. Using their data and their conversion of CO intensities to molecular gas surface densities, we calculated molecular gas densities. We then used the 850 μm flux densities, the dust temperatures, and the

associated emissivity assumptions used to fit the SEDs to calculate dust masses. Working at 850 μm is preferred because the determination of dust masses at that wavelength is relatively insensitive to uncertainties in dust temperatures. With these masses, we then calculated gas-to-dust ratios that may be compared to the Milky Way ratio.

4.1. Dust Masses and Gas-to-Dust Mass Ratios

We calculated dust masses using

$$M_{\text{Dust}} = \left[\frac{F(\nu) D^2}{B(\nu, T)} \right] \left[\frac{4a}{3Q(\nu)} \right] \rho, \quad (6)$$

derived in Hildebrand (1983). M_{Dust} is the dust mass, $F(\nu)$ is the measured flux density, D is the distance, $B(\nu, T)$ is the flux density from a blackbody of temperature T , a is the approximate average size of an interstellar dust grain, $Q(\nu)$ is the emissivity, and ρ is the density of a dust grain. Since these are nearby spiral galaxies, we assume that these galaxies contain dust with properties similar to the dust in the Milky Way. Therefore, we have also used the assumptions in Hildebrand (1983) for calculating dust masses. The size and density of the dust grains are assumed to be $a = 0.1 \mu\text{m}$ and $\rho = 3 \text{ g cm}^{-3}$. For the emissivities, we use the expression

$$Q(\lambda, \beta) = Q_0 a (250/\lambda)^\beta \quad (7)$$

from Klaas et al. (2001), where $Q_0 = 40 \text{ cm}^{-1}$ and β is the

TABLE 8
GLOBAL DUST MASSES AND GAS-TO-DUST RATIOS

GALAXY	DUST MASSES (M_{\odot})			MOLECULAR GAS MASSES (M_{\odot})	GAS-TO-DUST RATIOS		
	λ^{-1} Emissivity	λ^{-2} Emissivity	$\lambda^{-\beta}$ Emissivity		λ^{-1} Emissivity	λ^{-2} Emissivity	$\lambda^{-\beta}$ Emissivity
NGC 4088.....	4.8×10^6	5.7×10^7	4.6×10^6	1.5×10^9	310	26	330
NGC 4414.....	1.3×10^6	1.2×10^7	2.6×10^6	1.5×10^9	1200	130	580
NGC 4631.....	1.4×10^6	2.1×10^7	1.4×10^6	4.4×10^8	310	21	310
NGC 4826.....	2.7×10^5	2.7×10^6	4.5×10^5	1.8×10^8	670	67	400
NGC 5236.....	3.5×10^5	2.0×10^6	1.7×10^6	9.5×10^8	2700	480	560
NGC 5713.....	5.5×10^6	6.5×10^7	9.3×10^6	3.0×10^9	550	46	320
NGC 5907.....	6.2×10^6	5.9×10^7	5.2×10^6	7.8×10^8	130	13	150

emissivity coefficient. This equation gives $Q(850 \mu\text{m}, 1) = 1.2 \times 10^{-4}$ and $Q(850 \mu\text{m}, 2) = 3.5 \times 10^{-5}$.

Table 8 lists the global dust masses calculated from the data in Tables 1, 5, 6, and 7. Dust masses calculated with steeper emissivity laws are always higher than those calculated with shallower emissivity laws for two reasons. First, the fits to the SED using the shallower emissivity function produce higher temperatures than those fits using the steeper emissivity functions. These higher temperatures lead to higher values of $B(\nu, T)$, which then result in lower calculated dust masses. The second is the difference in the dust grain emissivity values at $850 \mu\text{m}$. The emissivity is higher for shallower emissivity functions, which leads to lower calculated dust masses. Essentially, a higher temperature or a higher emissivity requires less dust to produce the measured submillimeter flux.

Table 8 also presents global molecular gas masses calculated from the data in Young et al. (1995) and the resulting global gas-to-dust mass ratios. (We did examine gas-to-dust ratios for separate nuclear and disk regions, but the comparison showed no clear distinction between nuclear and disk ratios.)

4.2. Discussion

Inspection of Table 8 shows that the gas-to-dust ratios ultimately depend on the emissivity function used to fit the data. Perhaps even more importantly, when the emissivity coefficient is fixed (i.e., proportional to λ^{-1} or λ^{-2}), the range of gas-to-dust ratios for these eight galaxies varies by factors of 20–30. With the λ^{-1} emissivities, the ratios range from 130 to 2700, and with the λ^{-2} emissivities and two temperature components, the ratios range from 13 to 480. However, when the emissivity coefficient is fitted to the data, the gas-to-dust ratios vary from 150 to 580, only a factor ~ 4 .

We may check the plausibility of these calculated gas-to-dust ratios using the Milky Way ratio as a benchmark. The molecular gas-to-dust ratio in the Milky Way has been determined to be 115 using *COBE* data (Sodroski et al. 1994). The median gas-to-dust ratio for the λ^{-1} emissivity fits is approximately a factor of 6 higher than the ratio for the Milky Way, so the single blackbody with the λ^{-1} emissivity is unlikely to accurately represent the physical conditions of the dust. The median ratio from the λ^{-2} emissivity fit is within a factor of 3 of the Milky Way value, so these fits are more plausible. The median ratio from the $\lambda^{-\beta}$ emissivity fits is also within a factor of 3, so these fits are equally plausible. Dale & Helou

(2002), however, have demonstrated empirically that fitting one or two blackbodies to far-infrared and submillimeter data may lead to underestimates of the dust mass by as much as a factor of 10 when compared with more realistic models that fit a series of blackbodies to the data. If we accept that this effect is present, the λ^{-1} and $\lambda^{-\beta}$ emissivity fits would produce gas-to-dust ratios near the Milky Way's, but the λ^{-2} emissivity ratios would be much too low to be plausible.

However, the range in ratios provides an additional criterion for comparing the three fits. The dust masses computed using both the λ^{-1} emissivity and the two-component model with very cold dust give gas-to-dust ratios that vary from galaxy to galaxy by factors of 20 and 37, respectively. In contrast, the range in the ratios for the $\lambda^{-\beta}$ fits is less than a factor of 4. Since these are all nearby spiral galaxies, we would expect the basic properties of the interstellar medium to be similar. If the best description of the dust is the one that gives the lowest dispersion in the gas-to-dust ratios, and gas-to-dust ratios that are similar to that for the Milky Way, then the $\lambda^{-\beta}$ emissivity fits are clearly preferred. The fits with the fixed emissivities give implausible variations in the gas-to-dust ratios, while the $\lambda^{-\beta}$ fits give a more acceptable range.

As a result, using both closeness to the Milky Way gas-to-dust ratio and the small dispersion of the ratios as an indication of the plausibility for the gas-to-dust ratios, it is evident that the fits using the $\lambda^{-\beta}$ emissivity, i.e., the right-hand column of Table 8, provide results that are most likely to be correct for the galaxies in this sample.

We are now able to address the larger question of the lack of consensus in the dust temperatures and even the number of different temperature components in normal galaxies that was described in § 1. It is clear from the analysis above that one can fit SEDs from 60–850 μm equally well by (1) a single temperature component with emissivity proportional to λ^{-1} , (2) a single temperature component with emissivity proportional to $\lambda^{-\beta}$, or (3) two temperature components, one of which is “cold,” with a temperature ~ 15 K, and the other with temperature ~ 30 K. This range of results is just what one finds in reviewing the literature on this subject over the past 20 yr. We suggest it is the assumptions made about the emissivity function in different studies that have largely produced the wide range of conclusions about the dust temperatures and dust masses in galaxies and the lack of consensus that has plagued this subject. We have shown that the assumptions most commonly used lead to implausible gas-to-dust ratios. The distinguishing feature of this

study is that we have tested the physical plausibility of various possible emissivity functions rather than adhering rigidly to an assumed emissivity function and calculating dust temperatures and other parameters.

As a result, having shown that the $\lambda^{-\beta}$ emissivity fits to the SEDs imply more plausible dust masses and gas-to-dust ratios than the other choices, what is the physical interpretation of this result? First, we note that in this model we use only one temperature component to approximate the dust emission when there is almost certainly a range of dust temperatures both within star formation regions and in the diffuse interstellar medium. Does this make sense? A priori, a two-component model might be more reasonable, since a warmer component from star formation regions and a cooler component from dust heated by the diffuse interstellar radiation field are expected. Since such models appear to result in dust masses that are too large and gas-to-dust ratios than are implausibly small, this suggests that the colder component in such models is a less significant contributor than the two-component fits imply. Since only a single temperature gives plausible dust masses, we suggest that if a second cold component to the dust emission from the diffuse interstellar medium is present, it is relatively insignificant in terms of both its contributions to the mass and to the SED. To distinguish its contribution apparently requires better spectral coverage and photometric precision in the submillimeter and millimeter regions than has been available heretofore.

We must also consider the physical interpretation of a variable emissivity law due to the varying β we find for this galaxy sample. The emissivity functions should be related to the average physical properties of the dust, such as the composition and grain size distribution, and these are expected to be relatively constant among nearby spiral galaxies. Is it not inconsistent to argue that the emissivity functions can vary when we also argue that the gas-to-dust ratios should be similar among spiral galaxies? We suggest two plausible interpretations for this result. First, it may be that the grain properties do vary among these galaxies. Dale & Helou (2002) and references therein present data that demonstrate how β may depend on environment. However, they argue that β should decrease as the temperature of dust increases, which is the opposite of the trend we have found. Instead, we suggest that galaxies that have undergone significant recent star formation activity and concomitant supernovae may have a somewhat altered dust grain population. Supernova shock waves can break down silicate grains with carbon mantles into individual silicate and graphite grains. Silicate grains have different emissivities than the graphite grains, so the average emissivity would change. Furthermore, the destruction of very large grains would make the emissivity function steeper. Breaking down the dust with supernova shock waves also suggests some dust grain destruction (Dyson & Williams 1997), which is exactly what is seen in these results for galaxies with steep emissivities. An alternative interpretation might be that the varying emissivity function is simply a second fitting parameter, in addition to a temperature, and this combination better accounts for the range of dust temperatures and other dust properties that are found in spiral galaxies.

5. CONCLUSIONS

We have shown that, for the 71 galaxies in the *ISO* Atlas sample, the 60–180 μm SEDs have mean temperatures of 31 K for the λ^{-1} emissivities and 25 K for the λ^{-2} emissivities. The blackbodies with λ^{-1} emissivities generally fit the data better than the ones with λ^{-2} emissivities. Analysis of the dust temperatures as a function of morphological type reveals that spirals from Sa-Scd have remarkably uniform dust temperatures that are virtually identical within the errors. Dust temperatures are enhanced above the average for the spirals only in E/SO galaxies and in galaxies with especially strong star formation activity. Data based on SEDs over this spectral range do not support the existence of a substantial cold component at a temperature less than 20 K in a large fraction of spiral galaxies, in contrast to some earlier studies.

For the eight galaxies in the sample with the SEDs measured from 60–850 μm , we showed that the 60–850 μm SEDs could be fitted equally well by (1) a single temperature component with emissivity proportional to λ^{-1} , (2) a single temperature component with emissivity proportional to $\lambda^{-\beta}$, or (3) two temperature components, one of which is “cold,” with a temperature ~ 15 K. We suggest that the enormous variation in reported dust temperatures and dust masses that characterize the literature on spiral galaxies is largely a reflection of the variety of assumptions for the emissivity functions employed.

To choose among these three assumptions, we used the gas-to-dust ratio as a criterion. Only the temperatures derived using the single temperature component with emissivity proportional to $\lambda^{-\beta}$ produced gas-to-dust ratios within a rather narrow range and one that was close to the gas-to-dust ratio for the Milky Way. We suggest that these results are most likely to represent the actual dust properties of normal spiral galaxies. In particular, we find the wide range in inferred gas-to-dust ratios derived with the assumption of a “cold” dust component less physically plausible than those ratios derived using a single temperature component with temperatures derived using $\lambda^{-\beta}$, with β calculated for each galaxy.

G. J. B. would like to thank Iain Coulson and Loretta Dunne for their help with the submillimeter observations and data processing, Daniel A. Dale for his comments on this paper, and the staff of *IRAS* for providing the HIRES data. The ISOPHOT data presented in this paper were reduced using PIA, which is a joint development by the ESA Astrophysics Division and the ISOPHOT Consortium with the collaboration of the Infrared Processing and Analysis Center. Contributing ISOPHOT Consortium institutes are DIAS, RAL, AIP, MPIK, and MPIA. The JCMT is operated by the Joint Astronomy Center on behalf of the UK Particle Physics and Astronomy Research Council, the Netherlands Organization for Scientific Research, and the Canadian National Research Council. This research has been supported by NASA grants NAG 5-3370 and JPL 961566.

REFERENCES

- Bendo, G. J., et al. 2002, *AJ*, 123, 3067 (Paper I)
- Braine, J., Krügel, E., Sievers, A., & Wielebinski, R. 1995, *A&A*, 295, L55
- Chini, R., Kreysa, E., Krügel, E., & Mezger, P. G. 1986, *A&A*, 166, L8
- Chini, R., & Krügel, E. 1993, *A&A*, 279, 385
- Chini, R., Krügel, E., Lemke, R., & Ward-Thompson, D. 1995, *A&A*, 295, 317
- Clements, D. L., Andreani, P., & Chase, S. T. 1993, *MNRAS*, 261, 299
- Dale, D. A., & Helou, G. 2002, preprint (astro-ph/0205085)
- Dale, D. A., Helou, G., Contursi, A., Silbermann, N. A., & Kolhatkar, S. 2001, *ApJ*, 549, 215
- Désert, F.-X., Boulanger, F., & Puget, J. L. 1990, *A&A*, 237, 215
- de Vaucouleurs, G., de Vaucouleurs, A., Corwin, H. G., Jr., Buta, R. J., Paturel, G., & Fouqué, P. 1991, *Third Reference Catalogue of Bright Galaxies* (Berlin: Springer)
- Devereux, N. A., & Young, J. S. 1990, *ApJ*, 359, 42
- Dunne, L., & Eales, S. 2001, *MNRAS*, 327, 697
- Dunne, L., Eales, S., Edmunds, M., Ivison, R., Alexander, P., & Clements, D. L. 2000, *MNRAS*, 315, 115
- Dyson, J. E., & Williams, D. A. 1997, *The Physics of the Interstellar Medium* (2d ed.; Bristol: Inst. Phys. Pub.)
- Eales, S. A., Wynn-Williams, C. G., & Duncan, W. D. 1989, *ApJ*, 339, 859
- Gabriel, C., Acosta-Pulido, J., Heinrichsen, I., Morris, H., & Tai, W.-M. 1997, in *ASP Conf. Ser. 125, Astronomical Data Analysis Software and Systems VI*, ed. G. Hunt & H. E. Payne (San Francisco: ASP), 108
- Guélin, M., Zylka, R., Mezger, P. G., Haslam, C. G. T., & Kreysa, E. 1995, *A&A*, 298, L29
- Haas, M., Lemke, D., Stickel, M., Hippelein, H., Kunkel, M., Herbstmeier, U., & Mattila, K. 1998, *A&A*, 338, L33
- Hildebrand, R. H. 1983, *QJRAS*, 24, 267
- Hippelein, H., et al. 1996, *A&A*, 315, L82
- Holland, W. S., et al. 1999, *MNRAS*, 303, 659
- Jenness, T., & Lightfoot, J. F. 1998, in *ASP Conf. Ser. 145, Astronomical Data Analysis Software and Systems VII*, ed. R. Albrecht, R. N. Hook, & H. A. Bushouse (San Francisco: ASP), 216
- Kessler, M. F., et al. 1996, *A&A*, 315, L27
- Klaas, U., et al. 2001, *A&A*, 379, 823
- Krügel, E., Siebenmorgen, R., Zota, V., & Chini, R. 1998, *A&A*, 331, L9
- Laureijs, R. J. 1999, *Point Spread Function Fractions Related to the ISOPHOT C100 and C200 Arrays, Version 1.0* (Noordwijk: ESA)
- Laureijs, R. J., Herbstmeier, U., Abrahám, P., Klaas, U., & Lemke, D. 2000, in *ISO Beyond Point Sources*, ed. R. J. Laureijs, K. Leech, & M. F. Kessler (Noordwijk: ESA), 131
- Lemke, D., et al. 1996, *A&A*, 315, L64
- Popescu, C. C., Misiriotis, A., Kylafis, N. D., Tuffs, R. J., & Fishera, J. 2000, *A&A*, 362, 138
- Popescu, C. C., Tuffs, R. J., Völk, H. J., Pierini, D., & Madore, B. F. 2002, *ApJ*, 567, 221
- Radovich, M., Klaas, U., Acosta-Pulido, J., & Lemke, D. 1999, *A&A*, 348, 705
- Sakamoto, K. 1996, *ApJ*, 471, 173
- Sandage, A., & Tammann, G. A. 1987, *A Revised Shapley-Ames Catalog of Bright Galaxies* (2d ed.; Washington: Carnegie Inst.)
- Siebenmorgen, R., Krügel, E., & Chini, R. 1999, *A&A*, 351, 495
- Sievers, A. W., Reuter, H.-P., Haslam, C. G. T., Kreysa, E., & Lemke, R. 1994, *A&A*, 281, 681
- Smith, J. 1982, *ApJ*, 261, 463
- Sodroski, T. J., et al. 1994, *ApJ*, 428, 638
- Stark, A. A., Davidson, J. A., Harper, D. A., Pernic, R., Loewenstein, R., Platt, S., Engargiola, G., & Casey, S. 1989, *ApJ*, 337, 650
- Stickel, M., et al. 2000, *A&A*, 359, 865
- Young, J. S., et al. 1995, *ApJS*, 98, 219